Irreversible magnetization switching using surface acoustic waves

L. Thevenard,[1] J.-Y. Duquesne,[1] E. Peronne,[1] H. J. von Bardeleben,[1] H. Jaffres,[2] S. Ruttala,[2]
J-M. George,[2] A. Lemaître,[3] and C. Gourdon[1]

[1]*Institut des Nanosciences de Paris, Université Pierre et Marie Curie, CNRS, UMR7588, 4 place Jussieu, 75252 Paris, France*
[2]*Unité Mixte de Physique CNRS/Thales and Université Paris Sud 11, Route Départementale 128, 91767 Palaiseau, France*
[3]*Laboratoire de Photonique et Nanostructures, CNRS, UPR 20, Route de Nozay, Marcoussis, 91460, France*

An analytical and numerical approach is developed to pinpoint the optimal experimental conditions to irreversibly switch magnetization using surface acoustic waves (SAWs). The layers are magnetized perpendicular to the plane and two switching mechanisms are considered. In precessional switching, a small in-plane field initially tilts the magnetization and the passage of the SAW modifies the magnetic anisotropy parameters through inverse magnetostriction. The SAW triggers precession and, eventually, reversal. Using the micromagnetic parameters of a fully characterized layer of the magnetic semiconductor (Ga,Mn)(As,P), we show that there is a large window of accessible experimental conditions (SAW amplitude/wave-vector, field amplitude/orientation) allowing irreversible switching. As this is a resonant process, the influence of the detuning of the SAW frequency to the magnetic system's eigenfrequency is also explored. Finally, another—nonresonant—switching mechanism is briefly contemplated and found to be applicable to (Ga,Mn)(As,P): SAW-assisted domain nucleation. In this case, a small perpendicular field is applied opposite the initial magnetization and the passage of the SAW lowers the domain nucleation barrier.

PACS number(s): 73.50.Rb, 75.60.Jk, 75.78.−n, 75.50.Pp

I. INTRODUCTION

In a large number of ferromagnets, the coupling between strain and magnetization originates from the spin-orbit interaction. This coupling was shown early on to be maximum when elastic and magnetic resonance (precession) frequencies match.[1] This effect has been revisited in the light of spintronics applications in the past few years with compelling dynamic experiments in both magnetic semiconductors[2,3] and metals.[4] A first approach relies on the generation of picosecond acoustic pulses (longitudinal or transverse phonons). When coupled to the layer's magnons, magnetization precession may be triggered,[3] but it remains a fairly inefficient mechanism as the strain spectrum peaks quite high (20–30 GHz[5]), well above typical precession frequencies (0.5–10 GHz). Switching of a perpendicularly magnetized (Ga,Mn)(As,P) structure has recently been demonstrated using this technique,[6] but the effect was shown to originate from incoherent phonons (heat waves) and not from a magnetostrictive effect due to the high-frequency coherent phonons. Another route consists in generating strain through lower-frequency (<2 GHz) surface acoustic waves (SAWs). On in-plane magnetized systems, SAWs have been used to drive ferromagnetic resonance in thin Ni films,[4] or periodically switch magnetization between hard and easy axes in Co bars sputtered on GaAs.[7] Recent theoretical work has focused on the switching of in-plane terfenol nanomagnets subjected to stress,[8,9] but no experimental or theoretical work has been published on perpendicularly magnetized systems. These materials are, for instance, particularly relevant to high-density magnetic information storage technologies. We believe SAWs offer two main advantages for magnetization reversal compared to picosecond acoustics: their frequencies easily match precession frequencies, and the generated acoustic wave has a narrow bandwidth (a few megahertz), as opposed to the broadband spectrum in the former technique.

In this work, we address theoretically the irreversible magnetization reversal in perpendicularly magnetized layers using surface acoustic waves. We consider a realistic test system consisting of a thin (Ga,Mn)(As,P) layer—a magnetostrictive dilute magnetic semiconductor. Two possible mechanisms are considered, both relying on the transient modification of the magnetic anisotropy by the SAW. In precessional switching, the magnetization is pulled away from equilibrium by an in-plane field, and the SAW triggers a large angle precession of the magnetization, which may end up in a full reversal. In SAW-assisted domain nucleation, a small perpendicular field is applied opposite the initial magnetization, and the SAW is used to locally lower the domain wall (DW) energy, and thus initiate domain nucleation, leading to a full reversal.

II. DESCRIPTION OF THE SYSTEM

A. Generation of SAWs

SAWs are excited and detected by interdigital transducers (IDTs) on a piezoelectric layer[10,11] deposited on a magnetic thin film [see Fig. 1(a)]. We will for now limit ourselves to the case of a Rayleigh wave propagating along the [100] axis of a cubic crystal. The case of a wave propagating along [110] will be discussed in Sec. IV B. The only finite propagating strain wave components are then $\varepsilon_{xx}(x,z,t)$, $\varepsilon_{zz}(x,z,t)$, and $\varepsilon_{xz}(x,z,t)$ [details in Appendix B, the axes defined in Fig. 1(a)]. Their wavelength is given directly by the IDT period $\Lambda_R \approx 3$–5 μm for $f = 0.5$–1 GHz, and their dispersion-free velocity by the elastic constants of the material, $V_R = 2711$ m s^{-1}, with $\Lambda_R = V_R/f$. Their contribution, as a function of depth is plotted in Fig. 1(b). Two hypotheses may then be made if the magnetic layer is taken much thinner (<50 nm) than Λ_R: (i) the ε_{xz} component can be neglected, as its amplitude remains weak close to the surface, and (ii) the strain field can be considered constant along z. We will therefore take $z = 0$
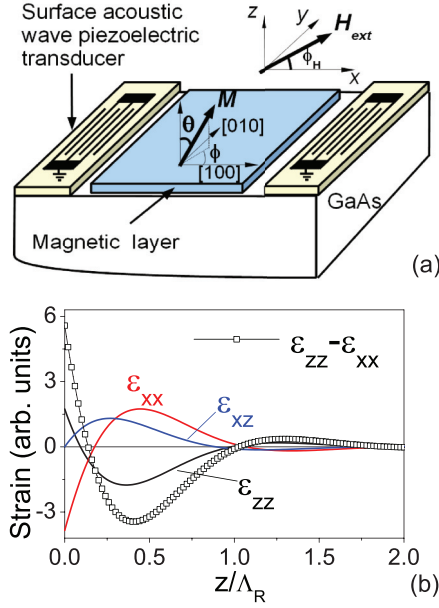
FIG. 1. (Color online) (a) Setup geometry for a SAW propagating along [100] and coordinates. (b) Depth dependence of the amplitude of the Rayleigh wave components ($f = 1$ GHz) plotted using Appendix B equations.

in the expressions of ε_{zz}, ε_{xx}, and $\varepsilon_{xz} = 0$. Finally, the RF power passing through the combs is small enough (10 mW) to neglect any resulting heating of the sample.

B. Magnetic system

The time-dependent dynamics of the magnetization are described by the Landau-Lifshitz-Gilbert (LLG) equation:

$$\frac{\partial \vec{M}}{\partial t} = -\gamma \vec{M} \times \mu_0 \vec{H}_{\text{eff}} + \frac{\alpha}{M_s} \vec{M} \times \frac{\partial \vec{M}}{\partial t}, \quad (1)$$

$$\mu_0 \vec{H}_{\text{eff}} = -\vec{\nabla}_M F(\vec{M}), \quad (2)$$

where $\vec{M}[\theta(x,t), \phi(x,t)]$ is the magnetization expressed in polar coordinates with M_s its norm (taken to be constant), $\gamma > 0$ is the gyromagnetic ratio and α is the damping constant. $\vec{H}_{\text{eff}}$ is the effective field, i.e., the sum of a magnetocrystalline anisotropy term, a shape anisotropy term, and finally the Zeeman contribution from the externally applied field. In this work (except in Sec. V), the exchange energy contribution will be neglected and we will effectively be looking at the behavior of a single macrospin.

Following Linnik *et. al*,[12] a normalized free energy density $F_M = F/M_s$ is defined, where F is a very general form of the free energy density of a cubic ferromagnetic layer distorted by strain:

$$
\begin{aligned}
&F_M(\theta, \phi) \\
&= (A_{2\varepsilon} - 2A_{4\varepsilon})\varepsilon(x,t)\cos^2\theta + (B_c + 2A_{4\varepsilon}\varepsilon(x,t))\cos^4\theta \\
&\quad + \frac{1}{4}\sin^4\theta(B_c - A_{4\varepsilon}\varepsilon(x,t))(3 + \cos 4\phi) \\
&\quad + \frac{\mu_0 M_s}{2}\cos^2\theta + \frac{1}{2}A_{2xy}\varepsilon_{xy}\sin^2\theta\sin 2\phi \\
&\quad - [\sin\theta(\mu_0 H_x\cos\phi + \mu_0 H_y\sin\phi) + \mu_0 H_z\cos\theta].
\end{aligned}
\quad (3)
$$

$\vec{H}_{\text{ext}} = (H_x, H_y, H_z)$ is the externally applied field and $\theta(x,t), \phi(x,t)$ is abbreviated into θ, ϕ. B_c is the cubic anisotropy field, and $A_{4\varepsilon}$, $A_{2\varepsilon}$, A_{2xy} are the magnetoelastic coefficients. The dependence of the magnetic anisotropy on strain is given through the terms ε_{xy} (static shear strain, details in Appendix A), and $\varepsilon(x,t) = \Delta\varepsilon_0 + \delta\varepsilon(x,t)$. $\delta\varepsilon(x,t) = \delta\varepsilon_{zz}(x,t) - \delta\varepsilon_{xx}(x,t)$ is the strain generated by the SAW. The Rayleigh wave propagating in a cubic material along $\vec{q}_\parallel$[100] has been calculated analytically, and found to slightly differ from the one used for isotropic materials (details in Appendix B). The resultant strain difference is given by[13]

$$\delta\varepsilon(x,t) = \varepsilon_{\max}\cos(\omega t - qx), \quad (4)$$

where $\varepsilon_{\max}$ is the SAW amplitude,[13] and q its wave vector, with $q = \omega/V_R$. $\Delta\varepsilon_0 = \varepsilon_{zz,0} - \varepsilon_{xx,0}$ is the difference between the static out-of-plane and in-plane strain components, related by the elastic modules C_{11}, C_{12} of GaAs[14] through $\varepsilon_{zz,0} = -2\frac{C_{12}}{C_{11}}\varepsilon_{xx,0}$.

III. ANALYTICAL SOLUTION: SMALL ANGLE PRECESSION

A. Principles of precessional switching

In so-called precessional switching, the perpendicular magnetization $\vec{M}$ is first tilted towards the layer by an in-plane magnetic field, which remains applied during the whole duration of the experiment. A short perturbation (e.g., an optical,[15,16] acoustic,[3] or ultra-fast magnetic[17] or electric[18] field pulse) then modifies the micromagnetic parameters enough to change the effective field seen by the magnetization, resulting in its precession. If the precession amplitude is sufficiently large, the magnetization can switch to another potential valley, where it will remain if the perturbation lasts an odd multiple of half the precession period,[17] or if damping eventually prevents $\vec{M}$ from oscillating between the two minima ("ringing" phenomenon). This mechanism has, for instance, been suggested for microwave assisted switching at a head field significantly below the medium coercivity[19] or for subnanosecond spin torque switching in magnetic tunnel junctions.[20]

The arrival of the SAW on the magnetic layer leads to a modification of the magneto-strictive anisotropy terms, and thereby of the effective field $\vec{H}_{\text{eff}}$. The time response of the magnetization is assumed short (around 100 ps) on the SAW's time scale, as evidenced by recent pump-probe experiments.[2] Equation (1) then shows that this triggers magnetization precession as long as the torque $\vec{M} \times \mu_0 \vec{H}_{\text{eff}}$ remains nonzero and the damping has not aligned $\vec{M}$ back along the effective field. Two computational approaches were then followed. Firstly, the conditions leading to magnetization precession were established by assuming small changes in magnetization direction, $\delta\theta$, $\delta\phi$, in order to solve this equation analytically. Secondly, in view of establishing the experimental conditions leading to irreversible precessional switching of a (Ga,Mn)(As,P) layer, the LLG equation was solved numerically, and a switching diagram established. In this work, perpendicularly magnetized layers were considered. This is often a problematic configuration, since the energy barriers are high for a full π reversal of the magnetization.

B. General solution

In this first approach, perturbations are small, leading to small changes in the magnetization direction around its equilibrium position $\vec{M}_0[\theta_0,\phi_0]$. Provided the magnetic anisotropy and in-plane applied fields are such that $\theta_0 \neq 0$, Eq. (1) can be linearized into

$$-\dot{\delta\theta} = \frac{\gamma}{\sin\theta_0}(F_{\phi\phi}\delta\phi + F_{\phi\theta}\delta\theta + F_{\phi\varepsilon}\delta\varepsilon) + \alpha\dot{\delta\phi}\sin\theta_0, \quad (5)$$

$$\dot{\delta\phi} = \frac{\gamma}{\sin\theta_0}(F_{\theta\theta}\delta\theta + F_{\theta\phi}\delta\phi + F_{\theta\varepsilon}\delta\varepsilon) + \frac{\alpha}{\sin\theta_0}\dot{\delta\theta}. \quad (6)$$

The terms F_{ij} stand for $\frac{\partial F_M}{\partial i \partial j}$, and the dot denotes the time derivative. In the following, the magnetization precession amplitude $\delta\theta(x,t)$ will be calculated in $x = 0$, but can easily be obtained at any distance x from the comb by computing $\delta\theta(t - x/V_R)$. When θ_0 is strictly zero, no precession can be observed, but SAW-induced domain nucleation may occur (see Sec. V).

The eigenfrequency of the system in the absence of acoustic wave is first determined by assuming harmonic solutions for the angle deviations: $\delta\theta = \delta\theta_0 e^{i\Omega_P t}$, $\delta\phi = \delta\phi_0 e^{i\Omega_P t}$. Expressing the determinant of the corresponding coupled equations system (5) and (6) then yields the complex precession frequency Ω_P of the magnetization in the presence of a finite damping term where we define $\Omega_P = \omega_P + i\chi$:

$$\omega_P = \frac{1}{\sqrt{1+\alpha^2}}\sqrt{\omega_0^2 - \frac{\alpha^2\gamma^2 H_\alpha^2}{4(1+\alpha^2)}}, \quad (7)$$

$$\chi = \frac{\alpha\gamma H_\alpha}{2(1+\alpha^2)}, \quad (8)$$

$$\omega_0 = \frac{\gamma}{\sin\theta_0}\sqrt{F_{\theta\theta}F_{\phi\phi} - F_{\theta\phi}^2}. \quad (9)$$

We have further defined an effective field $H_\alpha = F_{\theta\theta} + F_{\phi\phi}/\sin^2\theta_0$, and the precession rate ω_0 in the absence of damping. Assuming the SAW arrives at an instant $t = 0$, the method of variation of parameters then yields the amplitude of the magnetization precession $\delta\theta(t)$ as a function of the exciting SAW frequency ω and amplitude $\varepsilon_{\max}$, the precession frequency ω_P and the damping α:

$$\delta\theta(t) = \frac{\varepsilon_{\max}\Omega_\theta}{(1+\alpha^2)\sqrt{(\omega^2 - \omega_{\text{res}}^2)^2 + \Gamma^4}}$$
$$\times \left[f(\omega,\beta)\cos(\omega t + \eta) - \frac{\omega_0 e^{-\chi t}}{\sqrt{1+\alpha^2}}\cos(\omega_P t + \xi) \right], \quad (10)$$

where ξ and η are two phase shifts that depend on ω and the material's parameters. $f(\omega,\beta)$, β, and Ω_θ are defined in Appendix D. We further define

$$\omega_{\text{res}}^2 = \omega_P^2 - \chi^2, \quad (11)$$

$$\Gamma = \sqrt{2\omega_P\chi}. \quad (12)$$

ω_{res} is the resonance frequency of the system and Γ is related to the resonance broadening. This very general expression of the precession amplitude highlights two physical behaviors. The first one is that, as expected intuitively, the precession consists of a forced term oscillating at the excitation frequency ω, and a damped term at the eigenfrequency of the magnetic system ω_P. The second one is that the excitation frequency giving the largest amplitude is not exactly ω_P, but a slightly lower value, ω_{res}, which is a modified resonance frequency of the damped system in the small perturbation regime. Finally, a broadening term Γ prevents any divergence of the precession amplitude at resonance.

The amplitude of the precession is linear in $\varepsilon_{\max}$ and Ω_θ, which depends nontrivially on the magnetostrictive coefficients, the damping, and the applied field through the value of θ_0, ϕ_0 (full formula in Appendix D). We will see below that its expression can, however, be greatly simplified in some limiting cases.

C. Application to thin (Ga,Mn)(As,P) layers

The dilute magnetic semiconductor (Ga,Mn)(As,P) is a good test-bench material to investigate fast acoustics-induced magnetization switching. The carrier-mediated nature of its ferromagnetic phase results in a strong dependence of the magnetic anisotropy on the strain state of the layer, through the heavy- and light-hole band splitting.[21] For instance, Glunk *et al.*[22] have shown that the perpendicular uniaxial anisotropy term is proportional to both the out-of-plane strain coefficient ε_{zz} and the hole concentration p. Moreover, contrary to metals, typical precession frequencies of (Ga,Mn)(As,P) can be fairly low, of the order of the gigahertz in small magnetic fields.[5] This range matches the usual SAW frequency range. Finally, the damping parameter can be rather high in this material ($\alpha = 0.1$–0.3, see Refs. 23 and 24) compared to metals ($\alpha = 0.01$ in Ni$_{80}$Fe$_{20}$), which will limit ringing effects preventing irreversible switching. Whereas in metals, precessional switching is mainly governed by the precession of the magnetization around the demagnetizing field, in (Ga,Mn)(As,P) this process will be driven by the magnetocrystalline anisotropy since its magnetization at saturation is weak.

While Eq. (3) conveniently highlights the magnetostrictive terms, the following form of energy is more commonly used[25] to determine experimentally the anisotropy coefficients in (Ga,Mn)(As,P) (details in Appendix A for the correspondence between both energy forms):

$$F_M(\theta,\phi)$$
$$= -B_{2\perp}\cos^2\theta - \frac{1}{2}B_{4\perp}\cos^4\theta - \frac{1}{8}B_{4\parallel}\sin^4\theta(3+\cos 4\phi)$$
$$- B_{2\parallel}\sin^2\theta\sin^2\left(\phi - \frac{\pi}{4}\right) + \frac{\mu_0 M_s}{2}\cos^2\theta$$
$$- [\sin\theta(\mu_0 H_x\cos\phi + \mu_0 H_y\sin\phi) + \mu_0 H_z\cos\theta]. \quad (13)$$

The magnetic anisotropy is largely dominated by the uniaxial term $B_{2\perp}$, followed by the cubic terms $B_{4\perp}$ and $B_{4\parallel}$, which result from the tetragonal distortion of the lattice as the magnetic layer grows strained upon its substrate. A linear dependence of the uniaxial anisotropy on strain has indeed been found experimentally using various techniques.[22,26,27] The in-plane uniaxial term $B_{2\parallel}$ is weakest and corresponds to a minor anisotropy between [110] and [1$\bar{1}$0] axes (details in Appendix A and Refs. 21 and 28).

To estimate quantitatively the amplitude of the precession, a sample of relatively weak perpendicular anisotropy is

chosen in order to have gigahertz or subgigahertz precession frequencies, adapted to SAWs excited by micrometer-wide IDTs. An existing 50-nm-thick sample, with a static strain $\varepsilon_{zz,0} = -0.05\%$ and $x_{Mn} \approx 7\%$ is considered. This small lattice mismatch, yielding a moderate magnetic anistropy, is obtained by alloying the (Ga,Mn)As layer with phosphorus ($y_P \approx 4\%$) as described in Ref. 29. At 95 K, $M_s = 9$ kAm^{-1} and ferromagnetic resonance spectroscopy yields: $B_{2\perp} = 19$ mT, $B_{4\perp} = 4$ mT, $B_{4\parallel} = 1$ mT, and $B_{2\parallel} = -1.2$ mT. The damping will be taken as $\alpha = 0.1$, but note that this term has been shown to vary between 0.001 and 0.3 with magnetic and electric doping, as well as whether one measures the extrinsic damping or an intrinsic Gilbert damping.[23,24,30]

Let us first put some numbers on the relevant frequencies ($f_k = \omega_k/2\pi$). Under an in-plane magnetic field of 2 mT ($\theta_0 = 3°$), Eqs. (7)–(9) and (11) yield $f_0 = 1.017$ GHz, $f_P = 1.007$ GHz, and $f_{res} = 1.002$ GHz. The resonance frequency decrease due to the inclusion of damping is therefore relatively small, a mere 1.5%. The broadening is rather average: 90 MHz (full width at half maximum). Finally, the transient oscillatory regime occurs on a time scale of $1/\chi = 1.6$ ns.

In order to isolate the relevant parameters to obtain a large angle precession at resonance, Ω_θ and $f(\omega_{res}, \beta)$ may be simplified provided the explicit energy density of (Ga,Mn)(As,P) [see Eq. (13)] is used and a few hypotheses are made. When the applied field does not saturate the magnetization into the plane, $\tan \beta \approx \beta < 1$ (see Appendix D), so we develop $f(\omega_{res}, \beta) \approx \omega_P + \chi\beta$. We verified numerically that this remains acceptable at saturation. We also use $A_{4\varepsilon} \ll A_{2\varepsilon}$,[13] $\alpha \ll 1$, and consider that ϕ_0 closely follows the applied field direction ϕ_H, so that $\mu_0 H_x \cos \phi_0 + \mu_0 H_y \sin \phi_0 \approx \mu_0 H_{ext}$. The precession amplitude at resonance can then be simplified into

$$|\delta\theta|_{max} \approx \varepsilon_{max} \frac{\Omega_{\theta,0}(\omega_P + \chi\beta)}{\Gamma^2}, \Omega_{\theta,0}$$

$$\approx \frac{4\gamma^2}{\omega_0} A_{2\varepsilon} \cos \theta_0 (B_{4\parallel} \sin^3 \theta_0 \cos 4\phi_0$$

$$- B_{2\parallel} \sin \theta_0 \sin 2\phi_0 + \mu_0 H_{ext}/2). \quad (14)$$

In Eq. (14), $A_{2\varepsilon}$ is roughly proportional to the uniaxial anisotropy term $B_{2\perp}$ (see Appendix A) while the in-plane anisotropy terms $B_{4\parallel}$ and $B_{2\parallel}$ are affine functions of $A_{2\varepsilon}$. One can see that a larger precession amplitude $|\delta\theta|_{max}$ first requires a large uniaxial anisotropy, and large in-plane anisotropies $B_{4\parallel}$ and $B_{2\parallel}$; but this will tend to increase the precession frequencies high above typical SAW frequencies for micrometer-sized IDTs. The applied field amplitude and angle can, however, also be optimized as we show in the following numerical calculations of $|\delta\theta|_{max}$ at fixed strain amplitude $\varepsilon_{max} = 10^{-5}$ (see Fig. 2). This value is taken deliberately small to remain in the small perturbation regime.

At fixed field amplitude $\mu_0 H_{ext} = 24$ mT (large enough to ensure $\phi_0 \approx \phi_H$, $\theta_0 = 47°$), the angle of the field is first varied in the plane [see Fig. 2(a)]. The precession amplitude is largest in the $\phi_H = 0$–90° range, with a maximum at $\phi_H = 45°$. This results from the competition between the two in-plane anisotropies terms maximized at $\phi_0 = 0°$ modulo 90° (for $B_{4\parallel} > 0$), or at $\phi_0 = 45°$ (for $B_{2\parallel} < 0$). The amplitude variations are, however, weak, and this is clearly not the most critical parameter. At fixed field angle $\phi_H = 0°$, the
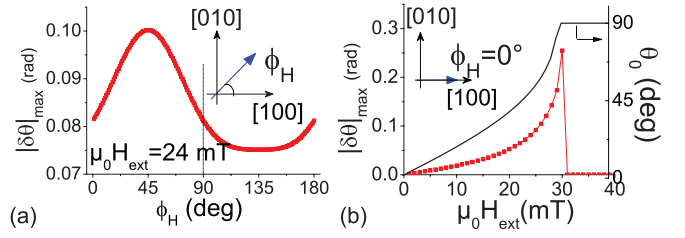

FIG. 2. (Color online) Conditions maximizing the precession amplitude at resonance in a perpendicularly magnetized (Ga,Mn)(As,P) layer for $\varepsilon_{max} = 10^{-5}$ using $|\delta\theta|_{max}$ in Eq. (14) and $\Omega_{\theta,0}$ in Eq. (22). (a) At fixed field intensity, variation of the precession amplitude as a function of the field angle ϕ_H. (b) At fixed field angle $\phi_H = 0°$, variation of the precession amplitude as a function of the field $\mu_0 H_{ext}$ (red symbols) compared to the tilt θ_0 (solid black line) before the arrival of the SAW.

precession amplitude is plotted as a function of the field intensity (and therefore of the initial tilt θ_0) in Fig. 2(b). The variations observed are this time more pronounced, and $|\delta\theta|_{max}$ is clearly maximum when the magnetization is most pulled away from its zero-field orientation. For fields above 30 mT, the magnetization is saturated in the plane, and the precession amplitude plummets down to a few 10^{-4} rad, and gradually decreases to zero. This sharp transition is linked to a brutal change in the amplitude and direction of the SAW-induced effective field variations ($\delta \vec{H}_{eff}$) from out-of-plane to mainly in-plane when $\cos \theta_0 = 0$ [see Eq. (3)]. It reflects the presence of a kink in the $\theta_0(H_{ext})$ curve at saturation [see Fig. 2(b)]. The precise variation of the precession amplitude with field intensity and orientation of course depends on the value of the anisotropy parameters. However, since ω_P, β, and Γ vary slowly with these parameters, the analytical dependence of $\Omega_{\theta,0}$ with ϕ_H and $\mu_0 H_{ext}$ given in Eq. (14) gives a good idea of the conditions maximizing this amplitude.

Finally, note that we have not taken into account the influence of the ferromagnetic resonance upon the acoustic wave propagation. We have indeed assumed the phonon-magnon coupling in (Ga,Mn)(As,P) sufficiently weak to neglect in first approximation the absorption of the acoustic wave upon interaction with the ferromagnetic layer. Please refer to Ref. 31 for a complete analytical treatment of this so-called "back-action" effect.

In summary, analytically solving the LLG equation in the presence of an SAW of given frequency has allowed us to identify the experimental parameters apt to yield the largest precession amplitude in a perturbative regime. The magnetic field should be as large as possible without saturating the layer and should be applied between [100] and [010] axes.

IV. NUMERICAL SOLUTION: IRREVERSIBLE PRECESSIONAL SWITCHING

A. Conditions for precessional switching

To explore the conditions for precessional switching, it is necessary to go beyond the small angle approximation and solve Eq. (1) numerically. The same sample as above is considered, with the field applied in the plane of the layer, along $\phi_H = 0°$.
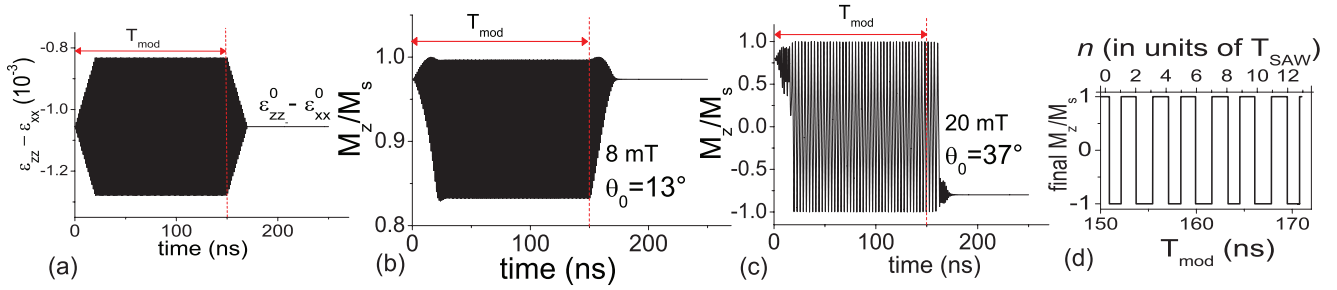
FIG. 3. (Color online) (a) Temporal profile of $\varepsilon(x = 0, t)$ for an rf burst of $T_{mod} = 150$ ns at $f_{SAW} = 800$ MHz, and a rise time $\tau = 20$ ns. Time behavior of the magnetization from numerical simulations for $\varepsilon_{max} = 2.10^{-4}$, $\alpha = 0.1$, $\delta f/f_P = 5\%$, $T_{mod} = 150$ ns and an initial magnetization pointing towards the upper half, $M_z/M_s \approx 1$. The field is applied along [100]. The SAW excitation time is indicated by the red dashed line. (b) Large angle precession. (c) Sustained switching leading to an irreversible reversal at the end of the SAW excitation. (d) Final magnetization state as a function of the SAW modulation time T_{mod}, under $\mu_0 H_{ext} = 20$ mT ($f_{SAW} = 646$ MHz, $1/f_{SAW} = 1.55$ ns).

Experimentally, SAWs can be excited by rf bursts of duration $T_{mod} \approx 150$ ns.[10] Here, we will only consider what happens during a single period. The rise time τ of the signal is given directly by the transit time of the acoustic wave through the emitting IDT. For about 10 pairs of teeth working at subgigahertz frequencies, a realistic value is $\tau \approx 20$ ns. The time profile of $\varepsilon(x, t) = \Delta\varepsilon_0 + \delta\varepsilon(x, t)$ taking into account a linear rise and decay time is simulated as shown in Fig. 3(a). The SAW's linewidth is roughly given by $1/T_{mod} = 7$ MHz. Four main parameters can then be adjusted numerically to explore the different behaviors of the system: the SAW amplitude, ε_{max} (5×10^{-5}–10^{-3}), the in-plane magnetic field amplitude, which in turn controls the initial tilt of the magnetization θ_0, the detuning of the SAW frequency to the precession frequency $\frac{|f - f_P|}{f_P}$, and finally, the damping parameter α. Note that the in-plane magnetic field remains applied during the whole duration of the simulation. Of those parameters, the first two can easily be changed during an experiment. Note that the detuning can equally be defined with respect to f_{res}, as they are within 1% of each other.

At fixed SAW amplitude and damping, two distinct behaviors are observed. Examples are shown in Figs. 3(b) and 3(c), where the magnetization initially points upwards ($M_z/M_s \approx 1$) before the application of the field, and the precession frequency lies around $f_P \approx 650$–980 MHz for the fields investigated. At low field (8 mT), such that the initial magnetization is moderately tilted towards the plane [$\theta_0 = 13°$, Fig. 3(b)] the magnetization remains pointing up during the excitation, and precesses at f_{SAW} in a cone that is widest when the SAW has reached its stationary regime. At the SAW extinction, the magnetization returns to its initial position. This regime will be defined as "large angle precession." Indeed, the amplitude of this precession is about ten times larger than the one observed in precession triggered by a picosecond acoustic pulse:[2] the strain pulse amplitude at the precession frequency is weak in this technique.

At larger applied field (20 mT), the magnetization first precesses in the upper quadrant at f_{SAW}, fully switches to $M_z/M_s \approx -1$, and then oscillates between up and down positions at half the excitation frequency [see Fig. 3(c)]. More exactly, the tip of the magnetization vector makes a complicated figure of eight with downwards and upwards trajectories

crossing close to the layer plane. A fast Fourier transform also evidences even lower harmonics, corresponding in the time domain to a slight variation of the precession amplitude. At the end of T_{mod}, the SAW amplitude decreases linearly [see Fig. 3(a)], but the up-and-down switching continues for a few periods. It then abruptly dwindles down to a small amplitude precession, evidencing the highly nonlinear aspect of this mechanism. By adjusting T_{mod}, the magnetization can be released in the downwards position provided the SAW is switched off in the right [$n/f_{SAW}, (n + 1)/f_{SAW}$] window [see Fig. 3(d)] typically around 1.5-ns wide in this case. The optimal value of T_{mod} for reversal is quite experiment-dependent though, as it depends on both the decay time of the SAW (related to the number of teeth in the IDT), and to the magnetization damping α. This regime will be named "sustained switching, conditional reversal." It relies on the same mechanism as the precessional switching using tailored ultra-fast magnetic field pulse, which was used in garnets[17,32] but the lower precession frequencies make the adjustment of T_{mod} less constraining. Plotting the final magnetization state as a function of the SAW modulation time, T_{mod} [see Fig. 3(d)] shows that the transition between final "up" and "down" states is very abrupt, across less than 1 ps. We also see that the period converges towards $2T_{SAW}$ over some time, but that the up/down cycle time actually varies slightly from one period to the next. This is due to the same lower frequency component of the signal, which was mentioned above.

In between those two behaviors is a transition regime (not shown) where the magnetization undergoes quite a chaotic behavior, at times switching irreversibly before the end of the SAW. Finally, for an applied field saturating the magnetization in the plane of the sample ($\theta_0 = 90°$, not shown), the SAW induces a precession of $\vec{M}$ around the applied field, with an amplitude that decreases when the strength of the applied field increases.

A more thorough exploration of the parameter space is shown in Fig. 4(a). The SAW amplitude ε_{max} is varied in steps of 2×10^{-4} or 2×10^{-5}, the in-plane applied field in steps of 1 mT with $\phi_H = 0°$, and the frequency detuning is first fixed to 5%. The resulting diagram shows that the behavior of Fig. 3 is very generic, regardless of the SAW amplitude: a large amplitude precession regime at low fields (in black), a conditional switching regime at high fields (in gray),
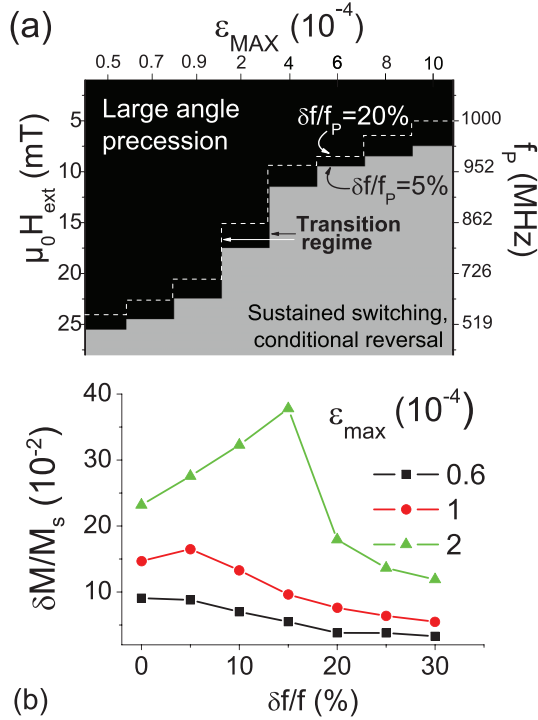
FIG. 4. (Color online) (a) Switching diagram of a macrospin excited by a SAW with $\alpha = 0.1$, an SAW frequency detuned by 5% from the precession frequency f_P, and an in-plane field along [100]. The large angle precession regime is separated from the sustained switching regime by the continuous white line (transition regime). Critical fields for a frequency detuning of 20% are indicated by the dashed line. (b) Amplitude of the precession $\frac{\delta M}{M_s}$ [Fig. 3(b) behavior] as a function of the detuning, for different strain amplitudes and $\mu_0 H_{ext} = 11$ mT.

and in between a transition regime (white line). As expected intuitively when ε_{max} decreases, the field necessary to obtain switching increases in order to keep the precession wide and compensate for this lesser efficiency. Note again that for large strain amplitudes, this generic behavior is maintained, but multiple frequencies appear in the sustained switching regime due to strong nonlinearities. The critical fields obtained for a larger detuning (20%) are indicated by the dashed line. Quite counterintuitively, these seem to be *lower* than the ones found for $\delta f/f = 5\%$, in particular, at higher strain amplitudes, as if a *larger* precession amplitude were obtained away from resonance as opposed to at resonance. To elucidate this, we set the field to 11 mT and systematically recorded the precession amplitude as a function of the frequency detuning, for three different strain amplitudes. The result is shown in Fig. 4(b), and confirms that whereas at low strain amplitude, the maximum precession amplitude is indeed obtained at resonance ($\delta f/f = 0\%$), when the strain amplitude increases, the maximum precession amplitude can be obtained quite far from resonance, at an increasingly large frequency detuning. This confirms that the small-perturbations approach of Sec. III is only valid for small strain amplitudes ($\varepsilon_{max} < 10^{-4}$), and that beyond, the behavior becomes highly nonlinear and the system's eigenfrequency is very probably not given by f_P anymore, but by a lower frequency. Finally, the main effect of

decreasing the damping (not shown) is to *lower* the critical field between large angle precession and precessional switching. The important conclusion of these simulations is that there is a large region of the (ε_{max}, $\mu_0 H_{ext}$) parameter space where irreversible switching of a macrospin is possible, and this at fairly low fields.

Note that a more elegant way of identifying switching conditions would be to determine an analytical criterion leading to the growth of nonlinearities in the system. This is not trivial in this coupled $\dot\theta = f(\phi, \theta, \dot\theta)$, $\dot\phi = g(\theta, \phi, \dot\phi)$ system and is beyond the scope of this paper.

B. Particular cases: (i) SAWs propagating along (110) and (ii) buried layers

Here we address the case of a Rayleigh wave propagating along a (110) direction, a configuration easier to implement experimentally. A straightforward calculation using a $\pi/4$ rotated frame shows that the SAW once again has three components, denoted ε_{XX}, ε_{ZZ}, and ε_{XZ}, of identical shape and similar amplitude as the one traveling along [100] (details in Appendix B). Given this strain tensor, we rotate it back into the $x \parallel [100]$ frame and inject the resulting components in the energy. The free energy density of the layer is then identical to Eq. (3) with $\varepsilon(x,t) = \Delta\varepsilon_0 + \varepsilon_{zz}(x,t) - \varepsilon_{xx}(x,t)$ replaced by $\Delta\varepsilon_0 + \varepsilon_{ZZ}(x,t) - \frac{1}{2}\varepsilon_{XX}(x,t)$, and $\varepsilon_{xy,0}$ replaced by $\varepsilon_{xy,0} \pm \frac{1}{2}\varepsilon_{XX}$ (+ for $\vec{q} \parallel [110]$, − for $\vec{q} \parallel [1\bar{1}0]$). The calculation therefore requires knowing $\varepsilon_{xy,0}$, which is problematic: there is no experimental measurement of this shear strain, and therefore no independent determination of A_{2xy} and $\varepsilon_{xy,0}$ is possible. We will therefore stick to the $\varepsilon_{xy,0} = 10^{-4}$ value used in Ref. 12, and deduce from our experimental value $B_{2\parallel} = -1.2$ mT the parameter $A_{2xy} = -12$ T.[13]

The amplitude of the precession triggered by the SAW is then estimated numerically using the same micromagnetic parameters as above. For strain amplitudes $\varepsilon_{max} = 0.5$ to 10×10^{-4}, and $\mu_0 H_{ext} = 5$ mT along [100], the precession amplitude when the SAW is traveling along [110] or [1$\bar{1}$0] is systematically about half the amplitude obtained when it travels along [100]. This is mainly due to the fact that the strain amplitude in front of the $A_{2\varepsilon}$ coefficient is reduced: the biaxial strain is along the crystallographic axes (100), and effectively reduced along the diagonals (110). The inverse magnetostrictive process is then less efficient.

Finally, we look at what happens for either a thick magnetic layer, or a buried layer, since the three Rayleigh wave strain components oscillate in amplitude with z [see Fig. 1(b)]. Away from the surface, ε_{zz} and ε_{xx} both reduce to their first zero within about 0.1–0.2Λ_{SAW}, whilst ε_{xz} takes over, albeit with a much smaller amplitude. For layers of this order of thickness (<300 nm in our case), the conclusions drawn above remain valid. However, an interesting case is that of a thin magnetic layer buried where ε_{xz} is maximum, and $\delta\varepsilon$ nonzero. As evidenced in Fig. 1(b), this lies around $z_c = 0.25\Lambda_{SAW}$, where $\delta\varepsilon$ is then still at about half its surface value.

In the (Ga,Mn)(As,P) free energy density form [see Eq. (13)], there is no dependence on ε_{xz} as this strain component is not present statically in the layers. However, just as a ε_{xy} term will give a magnetic anisotropy between [110] and [1$\bar{1}$0] axes [term $\frac{1}{2}A_{2xy}\varepsilon_{xy}\sin^2\theta\sin 2\phi$ in Eq. (3)],

it is easy to imagine that a ε_{xz} term will give a magnetic anisotropy between [110] and [001] axes, expressed as $\frac{1}{2}A_{2xz}\varepsilon_{xz}\sin 2\theta \cos\phi$. This term was evaluated numerically to $A_{2xz} = 80$ T (details in Appendix C) close to 95 K.

The amplitude of the magnetization precession triggered by the SAW was then compared at fixed applied field 5 mT, and SAW frequency 919 MHz (5% detuning) and strain amplitude $\varepsilon_{max} = 10^{-5}$ for a surface layer ($z = 0$) or for a layer buried at $z_c = 0.25\Lambda_{SAW}$. In the latter case, the precession amplitude is almost three times larger compared to a surface layer. This is due to the fact that A_{2xz} is large and that the three strain components now contribute to the precession. However, for the precession frequencies explored at 95 K, Λ_{SAW} is too large (about 3 microns at 5 mT), and z_c therefore unrealistically deep. This option might, however, prove more relevant for materials requiring higher SAW frequencies (smaller Λ_{SAW}).

V. SAW ASSISTED DOMAIN NUCLEATION

Let us mention briefly another approach for irreversible switching induced by an SAW. More likely than the (coherent) precessional switching of a structure, is the possibility that the SAW will locally lower a domain nucleation barrier and thus switch the whole layer under a small (propagating) magnetic field applied concurrently opposite to the initial magnetization. Indeed, in perpendicularly magnetized layers, the coercive field $\mu_0 H_c$ is largely determined by DW nucleation and/or propagation barriers.[33] Transient reduction of coercivity has already been demonstrated in garnets[34] or magnetic semiconductors[35,36] using ultrafast light pulses. It is also at the basis of thermomagnetic writing.

Neglecting the stray field energy between the nucleated domain and the rest of the layer,[37] the domain nucleation barrier can be expressed as $E_{nuc} = 2\pi r_{nuc} d\,\sigma$, where d is the layer thickness, r_{nuc} is the radius of the nucleated domain, and σ is its surface energy. The latter depends on the perpendicular uniaxial anisotropy and the exchange constant A_{ex} through $\sigma \propto \sqrt{A_{ex}B_\perp(\varepsilon_{xx},\varepsilon_{zz})}$.[37] If the magnetization reversal is nucleation limited, switching then occurs on a typical timescale given by the Arrhenius law $\tau = \tau_0 \exp(\frac{E_Z+E_{nuc}}{k_B T})$, where $k_B T$ is the thermal energy, and $E_Z = -\mu_0 H_{ext} M_s \times d\pi r_c^2$ is the Zeeman energy, which lowers this barrier, with H_{ext} the field applied perpendicular to the layer. τ_0 is the typical time needed for an energy exchange between spin and lattice, and depends on the damping, the anisotropy constants, and the magnetization.[38] It is usually estimated to about 10 ps.

For the sample at 95 K considered above, the effective uniaxial anisotropy field is $B_\perp \approx B_{2\perp} + B_{4\perp} = 23$ mT. Previous temperature dependent experiments on (Ga,Mn,As,P)[39] have moreover given $A_{ex} = 10^{-13}$ pJ/m, providing an estimation of the DW surface energy $\sigma = 2 \times 10^{-5}$ J/m². Experimental hysteresis loops done at 90 K yield $\mu_0 H_c = 2$ mT, with the perpendicular field applied in ≈ 100 ms pulses. Using the Arrhenius law, this gives an *experimental* estimation of the nucleated domain's diameter of a few nanometers. The nucleation barrier is then of the order of 44 meV (much lower than the intrinsic 1 eV barrier estimated using DW nucleation theory[23]), the Zeeman lowering around $-3 \times 10^{-2} H_{ext}$ meV/mT, while the thermal energy lies around 8 meV. In the presence of the SAW, the effective anisotropy coefficient

becomes $B_\perp^{SAW}(x,t) = (A_{2\varepsilon} - 2A_{4\varepsilon})[\Delta\varepsilon_0 + \delta\varepsilon(x,t)]$. Because the lattice mismatch is small in this sample (in order to have a weak anisotropy), the transient strain modification $\delta\varepsilon(x,t)$ can very well be of the order of the static strain mismatch $\Delta\varepsilon_0$ [see Fig. 3(a)], thus strongly reducing the uniaxial anisotropy field. This dramatically lowers the DW nucleation barrier during about a quarter of the SAW's period. If the resulting switching time τ is shorter than the time during which this barrier is very low, ultrafast magnetization switching is expected to occur under a small (propagating) perpendicular field. Note that this is a nonresonant process, and as such does not involve any strong constraint on the SAW frequency. On the contrary, it might be more relevant to aim for low frequency, which will leave plenty of time for the domain to nucleate during the transient decrease of anisotropy.

VI. DISCUSSION

In the first approach (see Secs. III and IV), the calculations and simulations were done for a macrospin at a fixed distance from the combs. For an extended, single-domain structure (no exchange energy), the conclusions will remain identical as long as the shape anisotropy of the structure is not significantly different from the $\frac{\mu_0 M_s}{2}\cos^2\theta$ term of Eqs. (3) and (13). For micrometer-sized structures, and given the weak magnetization of (Ga,Mn)(As,P), this is legitimate. However, for samples with a strong shape anisotropy, a modified demagnetization factor would need to be included in the energy form, as was done by Roy *et al.*[8] A more proper solution would in fact eventually need to take into account the exchange contribution in the free energy. In both picosecond acoustic pulses- and SAW-induced precession, the modification of the eigenfrequencies due to this exchange contribution was shown to be negligible,[3,31] given the dispersion curve in the considered regime remains almost flat. An estimation of this contribution to the real space, i.e., the generation of spin waves to accommodate a spatially varying magnetization vector is a problem more appropriately tackled by micromagnetic finite elements methods, and is beyond the scope of this paper.

In the second approach, a phenomenological model of SAW-assisted domain nucleation is used where exchange is implicitly taken into account (formation of a domain wall), and the field applied perpendicularly to the plane. Once again, SAWs seem more adequate than picosecond acoustic pulses. Indeed, were the transient strain strong enough at the relevant frequency to induce a substantial change of the uniaxial anisotropy coefficient to lower the domain's nucleation barrier, this would only last about 10 ps,[5] which would require an ultra-fast DW nucleation. Looking at the Arrhenius law once again shows that this would mean effectively canceling the energy barrier, in order to have $\tau \approx \tau_0$, which seems unlikely given the weak accessible transient strain amplitudes in this technique.

VII. CONCLUSION

A general analytical approach to SAW-assisted magnetization precessional switching has been developed based on the strain dependence of the magnetic anisotropy coefficients, and taking the damping into account. Several parameters

were found to be relevant, such as a large in-plane field, and SAWs propagating along [100] rather than [110]. Numerical simulations using realistic experimental parameters of (Ga,Mn)(As,P) then clearly evidenced a wide range of fields and SAW amplitudes under which irreversible switching was possible. SAWs were shown to possibly be a more adequate method to switch magnetization than picosecond acoustic pulses. Finally, although these concepts were tested on (Ga,Mn)(As,P) thin films, the analytical forms of energy and precession amplitude given in this work make them applicable to any magnetostrictive material.

APPENDIX A: MAGNETIC ANISOTROPY COEFFICIENTS

The magnetic anisotropy terms $A_{4\varepsilon}$, $A_{2\varepsilon}$, A_{2xy}, and B_c of Eq. (3), and the terms $B_{2\perp}$, $B_{4\perp}$, $B_{2\parallel}$, and $B_{4\parallel}$ (obtained experimentally by ferromagnetic resonance experiments for instance) of Eq. (13) are related as follows:

$$A_{4\varepsilon} = \frac{B_{4\parallel} - B_{4\perp}}{6\Delta\varepsilon_0}, \quad A_{2\varepsilon} = \frac{B_{4\parallel} - B_{4\perp}}{3\Delta\varepsilon_0} + \frac{B_{2\parallel} - 2B_{2\perp}}{2\Delta\varepsilon_0},$$

$$B_c = -\frac{2B_{4\parallel} + B_{4\perp}}{6}, \quad A_{2xy} = \frac{B_{2\parallel}}{\varepsilon_{xy,0}},$$

where $\Delta\varepsilon_0 = \varepsilon_{zz,0} - \varepsilon_{xx,0}$.

For the vast majority of (Ga,Mn)(As,P) samples, the relationship $A_{4\varepsilon} \ll A_{2\varepsilon}$ holds.

Note that there is no experimental evidence of an $\varepsilon_{xy,0}$ shear strain, but rather it is a physical effect of the same symmetry that is at the root of the weak uniaxial anisotropy $B_{2\parallel}$. During the growth, when atoms are mobile on the surface, nearest-neighbor Mn pairs on the GaAs (001) surface have a lower energy for the [1−10] direction compared to the [110].[28]

APPENDIX B: DERIVATION OF THE STRAIN WAVE EXPRESSION

The strain components of the Rayleigh wave propagating in a cubic material along $\vec{q} \parallel [100]$ are slightly different from the usual formulas found in textbooks for isotropic materials. They can be found analytically as

$$\varepsilon_{xx}(r,z,t) = -2i\zeta_0 q e^{i\psi_2/2} e^{-aqz} \cos(bqz + \psi_2/2) e^{i(\omega t - \vec{q}\cdot\vec{r})},$$

$$\varepsilon_{zz}(r,z,t) = -2i\rho\zeta_0 q e^{i\psi_2/2} e^{-aqz}[-a\sin(bqz + \psi_2/2 - \psi_1)$$
$$+ b\cos(bqz + \psi_2/2 - \psi_1)] e^{i(\omega t - \vec{q}\cdot\vec{r})}$$

$$\varepsilon_{xz}(r,z,t) = -\zeta_0 q e^{i\psi_2/2} e^{-aqz}[a\cos(bqz + \psi_2/2)$$
$$+ b\sin(bqz + \psi_2/2) + \rho\sin(bqz + \psi_2/2 - \psi_1)]$$
$$\times e^{i(\omega t - \vec{q}\cdot\vec{r})}.$$

We define the wave vector $\vec{q}$ (norm q), the position $\vec{r}$ (norm r), and ζ_0 the amplitude of the displacement. When $\vec{q} \parallel (100)$, $\vec{q}\cdot\vec{r} = qx$ and for a magnetic layer much thinner than Λ_{SAW}, we can set $z = 0$ [see Fig. 1(b)], and simplify $\delta\varepsilon(x,t) = \varepsilon_{zz}(x,0,t) - \varepsilon_{xx}(x,0,t)$ into $\delta\varepsilon(x,t) = \varepsilon_{max}\cos(\omega t - qx)$, where ε_{max} is the amplitude of the resulting wave.

The parameters are related by $a\cos\psi_2/2 + b\sin\psi_2/2 = \rho\sin(\psi_1 - \psi_2/2)$. For GaAs and $\vec{q} \parallel (100)$, the values found numerically are $\psi_1 = -0.328$, $\psi_2 = -1.9$, $\rho = 1.18$, $a = 0.402$, and $b = -0.561$. For $\vec{q} \parallel (110)$, these coefficients are only slightly modified: $\psi_1 = -0.531$, $\psi_2 = -2.1$, $\rho = 1.34$, $a = 0.500$, and $b = -0.480$, yielding strain amplitudes about 15% smaller than along (100) directions.

APPENDIX C: EFFECT OF A ε_{xz} STRAIN COMPONENT ON MAGNETIZATION PRECESSION

In the presence of a ε_{xz} strain component, one can expect a magnetostrictive component[12] of the form $A_{2xz}\varepsilon_{xz}m_x m_z = \frac{1}{2}A_{2xz}\varepsilon_{xz}\sin 2\theta\cos\phi$. This term can be evaluated theoretically using an effective mass Hamiltonian with the six-band k·p Luttinger-Kohn term, a strain tensor, and the p-d exchange interaction of the holes and the Mn spins in the molecular-field approximation.[21,40] The saturation magnetization was set to 6 kA m^{-1} ($\approx$95 K), which corresponds to a $|B_G| = 3.5$ meV spin splitting parameter.[21] The usual biaxial strain terms $\varepsilon_{zz,0},\varepsilon_{xx,0}$ were set to zero, and a nonzero term $id\varepsilon_{xz}$ introduced in the Bir-Pikus strain tensor, where $d = -4.8$ eV is the shear deformation potential.[40] In this way, B_c and A_{2xz} were the only unknown parameters in the free energy density. The energy difference $F(\theta) - F([001]) = Bc(\cos^4\theta + \sin^4\theta) + \frac{1}{2}A_{2xz}\varepsilon_{xz}\sin 2\theta$ was then computed and fit numerically for $p = 3 \times 10^{20}$ cm^{-3} yielding $A_{2xz} = 80$ T. This value is quite large, in fact, larger than any of the anisotropy parameters, but the resulting anisotropy field expected to be less than 10 mT.

APPENDIX D: SMALL ANGLE MAGNETIZATION PRECESSION AMPLITUDE

The precession amplitude $\delta\theta$ given in Eq. (10) depends on various parameters given below:

$$f_\theta = -\frac{\gamma}{\sin\theta_0}F_{\phi\varepsilon_{zz}}, \tag{D1}$$

$$f_\phi = \frac{\gamma}{\sin\theta_0}F_{\theta\varepsilon_{zz}}, \tag{D2}$$

$$f(\omega,\beta) = \sqrt{\frac{\tan^2\beta}{1+\tan^2\beta}\left[\omega^2 + \left(\frac{\omega_P}{\tan\beta} + \chi\right)^2\right]}, \tag{D3}$$

$$\tan\beta = -\frac{\omega_P}{\gamma}\frac{2(1+\alpha^2)}{\alpha H_\alpha + \frac{2(1+\alpha^2)}{\sin\theta_0}\left(\frac{f_\theta F_{\theta\phi} + f_\phi F_{\phi\phi}}{f_\theta - f_\phi\alpha\sin\theta_0}\right)}, \tag{D4}$$

$$\Omega_\theta = -\sqrt{(f_\phi\alpha\sin\theta_0 - f_\theta)^2 + \frac{\{f_\phi\sin\theta_0[2F_{\phi\phi} + \alpha^2(F_{\phi\phi} - F_{\theta\theta}\sin^2\theta_0)] + f_\theta[\alpha H_\alpha\sin^2\theta_0 + 2F_{\theta\phi}\sin\theta_0(1+\alpha^2)]\}^2}{\sin^4\theta_0\left[(1+\alpha^2)\frac{4\omega_0^2}{\gamma^2} - \alpha^2 H_\alpha^2\right]}}. \tag{D5}$$

In the case of (Ga,Mn)(As,P), some approximations can be made using $A_{4\varepsilon} \ll A_{2\varepsilon}$ (which implies $f_\theta \ll f_\phi$) and developing Ω_θ to its zeroth order expansion in α:

$$f_\theta = -\gamma A_{4\varepsilon} \sin^3 \theta_0 \sin 4\phi_0, \qquad (D6)$$

$$f_\phi \approx -2\gamma A_{2\varepsilon} \cos \theta_0, \qquad (D7)$$

$$\Omega_{\theta,0} = -\sqrt{f_\theta^2 + \frac{(f_\theta F_{\theta\phi} + f_\phi F_{\phi\phi})^2 \gamma^2}{\sin^2 \theta_0 \omega_0^2}}. \qquad (D8)$$

[1] H. Bömmel and K. Dransfeld, Phys. Rev. Lett. **3**, 83 (1959).

[2] A. V. Scherbakov, A. S. Salasyuk, A. V. Akimov, X. Liu, M. Bombeck, C. Brüggemann, D. R. Yakovlev, V. F. Sapega, J. K. Furdyna, and M. Bayer, Phys. Rev. Lett. **105**, 117204 (2010).

[3] M. Bombeck, A. S. Salasyuk, B. A. Glavin, A. V. Scherbakov, C. Brüggemann, D. R. Yakovlev, V. F. Sapega, X. Liu, J. K. Furdyna, A. V. Akimov, and M. Bayer, Phys. Rev. B **85**, 195324 (2012).

[4] M. Weiler, L. Dreher, C. Heeg, H. Huebl, R. Gross, M. S. Brandt, and S. T. B. Goennenwein, Phys. Rev. Lett. **106**, 117601 (2011).

[5] L. Thevenard, E. Peronne, C. Gourdon, C. Testelin, M. Cubukcu, E. Charron, S. Vincent, A. Lemaître, and B. Perrin, Phys. Rev. B **82**, 104422 (2010).

[6] A. Casiraghi, P. Walker, A. V. Akimov, K. W. Edmonds, A. W. Rushforth, E. De Ranieri, R. P. Campion, B. L. Gallagher, and A. J. Kent, Appl. Phys. Lett. **99**, 262503 (2011).

[7] S. Davis, A. Baruth, and S. Adenwalla, Appl. Phys. Lett. **97**, 232507 (2010).

[8] K. Roy, S. Bandyopadhyay, and J. Atulasimha, Phys. Rev. B **83**, 224412 (2011).

[9] M. S. Fashami, K. Roy, J. Atulasimha, and S. Bandyopadhyay, Nanotechnology **22**, 155201 (2011).

[10] J.-Y. Duquesne, J.-Y. Prieur, J. A. Canalejo, V. H. Etgens, M. Eddrief, A. L. Ferreira, and M. Marangolo, Phys. Rev. B **86**, 035207 (2012).

[11] H. Sanada, T. Sogawa, H. Gotoh, K. Onomitsu, M. Kohda, J. Nitta, and P. V. Santos, Phys. Rev. Lett. **106**, 216602 (2011).

[12] T. L. Linnik, A. V. Scherbakov, D. R. Yakovlev, X. Liu, J. K. Furdyna, and M. Bayer, Phys. Rev. B **84**, 214432 (2011).

[13] See Appendixes for the full derivation.

[14] Some very nice temperature dependent experiments have actually derived C_{11} for GaMnAs [Qi *et al.*, Phys. Rev. B **81**, 115208 (2010)], but not C_{12}, so we will keep the GaAs values.

[15] A. V. Kimel, A. Kirilyuk, A. Tsvetkov, R. V. Pisarev, and T. Rasing, Nature (London) **429**, 850 (2004).

[16] J. A. de Jong, I. Razdolski, A. M. Kalashnikova, R. V. Pisarev, A. M. Balbashov, A. Kirilyuk, T. Rasing, and A. V. Kimel, Phys. Rev. Lett. **108**, 157601 (2012).

[17] T. Gerrits, H. A. M. Van Den Berg, J. Hohlfeld, L. Bär, and T. Rasing, Nature (London) **418**, 509 (2002).

[18] P. Balestrire, T. Devolder, J.-V. Kim, P. Lecoeur, J. Wunderlich, V. Novak, T. Jungwirth, and C. Chappert, Appl. Phys. Lett. **99**, 242505 (2011).

[19] J.-G. Zhu, X. Zhu, and Y. Tang, IEEE Trans. Magn. **44**, 125 (2008).

[20] G. E. Rowlands, T. Rahman, J. A. Katine, J. Langer, A. Lyle, H. Zhao, J. G. Alzate, A. A. Kovalev, Y. Tserkovnyak, Z. M. Zeng, H. W. Jiang, K. Galatsis, Y. M. Huai, P. K. Amiri, K. L. Wang, I. N. Krivorotov, and J.-P. Wang, Appl. Phys. Lett. **98**, 102509 (2011).

[21] T. Dietl, H. Ohno, and F. Matsukura, Phys. Rev. B **63**, 195205 (2001).

[22] M. Glunk, J. Daeubler, L. Dreher, S. Schwaiger, W. Schoch, R. Sauer, W. Limmer, A. Brandlmaier, S. T. B. Goennenwein, C. Bihler, and M. S. Brandt, Phys. Rev. B **79**, 195206 (2009).

[23] C. Gourdon, A. Dourlat, V. Jeudy, K. Khazen, H. J. von Bardeleben, L. Thevenard, and A. Lemaître, Phys. Rev. B **76**, 241301 (2007).

[24] P. Němec, V. Novák, N. Tesařová, E. Rozkotová, H. Reichlová, D. Butkovičová, F. Trojánek, K. Olejník, P. Malý, R. P. Campion, B. L. Gallagher, J. Sinova, and T. Jungwirth, Nat. Commun. **4**, 1422 (2013).

[25] M. Farle, Rep. Prog. Phys. **61**, 755 (1998).

[26] S. C. Masmanidis, H. X. Tang, E. B. Myers, M. Li, K. De Greve, G. Vermeulen, W. V. Roy, and M. L. Roukes, Phys. Rev. Lett. **95**, 187206 (2005).

[27] M. Cubukcu, H. J. von Bardeleben, K. Khazen, J. L. Cantin, O. Mauguin, L. Largeau, and A. Lemaître, Phys. Rev. B **81**, 041202(R) (2010).

[28] M. Birowska, C. Śliwa, J. A. Majewski, and T. Dietl, Phys. Rev. Lett. **108**, 237203 (2012).

[29] A. Lemaître, A. Miard, L. Travers, O. Mauguin, L. Largeau, C. Gourdon, V. Jeudy, M. Tran, and J.-M. George, Appl. Phys. Lett. **93**, 21123 (2008).

[30] K. Khazen, H. J. von Bardeleben, M. Cubukcu, J. L. Cantin, V. Novak, K. Olejnik, M. Cukr, L. Thevenard, and A. Lemaître, Phys. Rev. B **78**, 195210 (2008).

[31] L. Dreher, M. Weiler, M. Pernpeintner, H. Huebl, R. Gross, M. S. Brandt, and S. T. B. Goennenwein, Phys. Rev. B **86**, 134415 (2012).

[32] M. Bauer, R. Lopusnik, J. Fassbender, and B. Hillebrands, Appl. Phys. Lett. **76**, 2758 (2000).

[33] E. du Tremolet de la Lacheisserie, *Magnetism: Fundamentals*, 1st ed. (Springer, New York, 2006).

[34] J. Hohlfeld, T. Gerrits, M. Bilderbeek, T. Rasing, H. Awano, and N. Ohta, Phys. Rev. B **65**, 012413 (2001).

[35] A. H. M. Reid, G. V. Astakhov, A. V. Kimel, G. M. Schott, W. Ossau, K. Brunner, A. Kirilyuk, L. W. Molenkamp, and T. Rasing, Appl. Phys. Lett. **97**, 232503 (2010).

[36] K. C. Hall, J. P. Zahn, A. Gamouras, S. March, J. L. Robb, X. Liu, and J. K. Furdyna, Appl. Phys. Lett. **93**, 32504 (2008).

[37] A. Hubert and R. Schäfer, *Magnetic Domains* (Springer, Berlin, 2000).

[38] C. H. Back, Science **285**, 864 (1999).

[39] S. Haghgoo, M. Cubukcu, H. J. von Bardeleben, L. Thevenard, A. Lemaître, and C. Gourdon, Phys. Rev. B **82**, 041301(R) (2010).

[40] J. Zemen, J. Kučera, K. Olejník, and T. Jungwirth, Phys. Rev. B **80**, 155203 (2009).